Floquet generation of a magnonic NOON state

Shi-fan Qi and Jun Jing [*]

School of Physics, Zhejiang University, Hangzhou 310027, Zhejiang, China

We propose a concise and deterministic protocol to generate NOON states in a hybrid system consisting of a superconducting qubit, a circuit resonator mode, and two magnonic modes, based on Floquet engineering. In particular, we construct a time-reversal-symmetry broken Hamiltonian for chiral state propagation of the three continuous-variable modes depending on qubit state, by the time modulation over qubit-resonator interaction and magnon frequency. Then, an arbitrary magnonic NOON state can be generated by a typical preparing-and-measurement procedure. We analyze the robustness of our protocol against the systematic errors in the qubit-magnon coupling strength, the Floquet-driving intensity, the frequency mismatch of the magnons, and the counterrotating interactions. We can obtain a high-fidelity NOON state in the presence of quantum dissipation on all components.

I. INTRODUCTION

NOON states, i.e., $(|N0\rangle + |0N\rangle)/\sqrt{2}$ with N integer, consisting of two symmetric components in the maximal superposition [1] constitute a prominent class of highly entangled states [2]. They offer diversified applications in quantum metrology [3], quantum communication [4], and quantum information processing [5]. The NOON-state generation protocols [6–15] are conventionally developed on various Rabi oscillations. They have been realized in multiple quantum platforms, such as polarization states of photons [16], nuclear spin of molecules [17], optical paths of photons [18], ultracold dipolar atoms in an optical superlattice setup [19,20], excitations in superconducting resonators [6,8], and phonons in ion trap [21]. The ultraprecise control over complex quantum devices and decoherence of quantum systems [22], however, makes it extremely difficult to create a NOON state with a large N. It therefore remains interesting to find fast and faithful approaches to generate NOON states in low-decoherence systems. Here, we propose to realize a magnonic NOON state by virtue of the chiral state transfer based on Floquet engineering.

The magnonic system is a growing field of research on magnetic devices that operate in the quantum realm. With unique properties such as high tunability, long coherent time, and strong dipole-dipole coupling to the microwave photons and qubits, magnonic modes have been used as the information carrier in an even broader variety of hybrid systems [23–25]. They are thus capable to prepare and manipulate various nonclassical states [26–34]. Bell states of the magnon-photon system can be observed in both theory proposal [35] and experimental demonstration [36]. Analogous to the cavity quantum electrodynamics [37], Ref. [38] proposed a magnonic cat-state generation protocol, in which the magnon

was directly and quantum-coherently coupled to a superconducting transmon qubit.

In a broader view, NOON states could be categorized with the nonclassical states in a (nonnormalized) form of $|\varphi\rangle|0\rangle + |0\rangle|\varphi\rangle$, where $|\varphi\rangle$ is an arbitrary pure state. They can result from a chiral state transfer depending on the symmetrically superposed state of a two-state system in charge of control. Chirality [39,40] has been found to play an important role in the fractional quantum Hall effect [41] in the magnetic materials. It breaks the time reversal symmetry [42] and perfectly realizes directional state transfer [43,44]. In recent experiments [45,46] on superconducting circuits and qubits, a three-spin interaction with chirality is fabricated by specially designed Floquet driving. Floquet engineering by fast periodic modulation over the characteristic frequency of a quantum system is a major control approach to the desired effective Hamiltonian for the long-time dynamics of the system [47–50]. It has also been implemented to realize quantum switch [51], chiral ground state current [43], and quantum simulation [52].

In this work, we consider a hybrid qubit-resonator-magnon system upon a state-of-the-art device, in which the qubit is coupled to the resonator mode with time-modulated strength [43,53] and simultaneously coupled to two magnonic modes [38]. Floquet engineering is applied to the frequencies of the magnonic modes [54]. Using appropriate frequencies, intensities, and local phases in control, we can fabricate an effective time-reversal-symmetry broken Hamiltonian to ensure chiral state transfer among resonator and magnonic modes. The transfer direction depends on the state of the qubit. A magnonic NOON state can thus be generated upon preparing the resonator mode as a Fock state $|N\rangle$ [55].

The rest of this work is structured as follows. In Sec. II, we introduce the full Hamiltonian for a hybrid qubit-resonator-magnon system and then derive the effective Hamiltonian for a perfect chiral state transfer among the three continuous-variable components. In Sec. III, we discuss the systematic
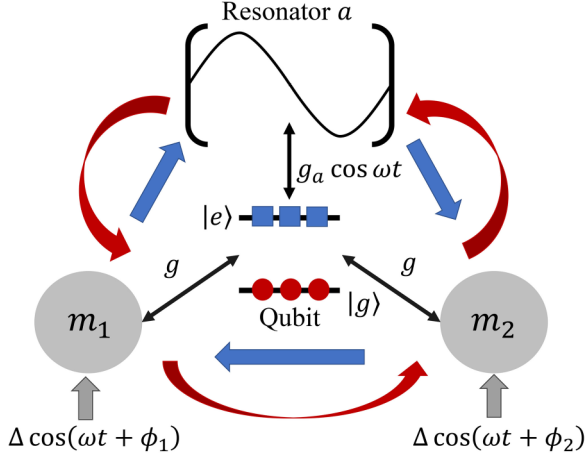
---

[*]jingjun@zju.edu.cn

FIG. 1. Diagram of the chiral state propagations among three continuous-variable modes a, m_1, and m_2 in a hybrid qubit-resonator-magnon system. The qubit population on the excited and ground states determines, respectively, the clockwise and anticlockwise directions of the chiral state propagation.

errors from the qubit-magnon coupling strength, the Floquet driving intensity, the frequency mismatch of the two magnonic modes, and the counterrotating interactions. The NOON-state generation protocol and its fidelity are analyzed in Secs. IV A and IV B, respectively. The whole work is summarized in Sec. V.

II. MODEL AND CHIRAL STATE TRANSFER

Consider a hybrid system that consists of a circuit resonator, a superconducting qubit, and two yttrium iron garnet (YIG) spheres in their ground states (the Kittel mode of the spin ensemble), as shown in Fig. 1. The transition frequencies of the qubit, resonator, and magnon mode k are supposed to be resonant with each other in the microwave regime, i.e., $\omega_q = \omega_a = \omega_k$. The qubit-resonator interaction and the frequencies of the two magnonic modes are under Floquet engineering [43,53,54]. Then, in the rotating frame with respect to the free Hamiltonian $H = \omega_a(\sigma^+\sigma^- + a^\dagger a + \sum_{k=1}^{2} m_k^\dagger m_k)$, the full Hamiltonian can be written as

$$H = g_a \cos(\omega t)(\sigma^+ a + \sigma^- a^\dagger) + \Delta \sum_{k=1}^{2} \cos(\omega t + \phi_k)m_k^\dagger m_k$$
$$+ g \sum_{k=1}^{2}(\sigma^+ m_k + \sigma^- m_k^\dagger), \quad (1)$$

where a ($a^\dagger$) and m_k ($m_k^\dagger$) are the annihilation (creation) operators for the resonator mode and the kth magnonic mode, respectively, and $\sigma^+ \equiv |e\rangle\langle g|$ and $\sigma^- \equiv |g\rangle\langle e|$ are Pauli transition operators. The qubit-resonator interaction is characterized by the coupling strength g_a and the driving frequency ω [43,53]. For magnons, Δ, ω, and ϕ_k represent the Floquet driving intensity, frequency, and local phases, respectively [54]. g is the qubit-magnon coupling strength [38]. The resonator-magnon interaction is vanishing when they depart with a significant distance.

In the rotating frame with respect to the magnon Hamiltonian under driving [the second term in Eq. (1)], we have

$$H(t) = g_a \cos(\omega t)(\sigma^+ a + \sigma^- a^\dagger)$$
$$+ g \sum_{k=1}^{2}(e^{if[\sin\phi_k - \sin(\omega t + \phi_k)]}\sigma^+ m_k + \text{H.c.}), \quad (2)$$

where $f \equiv \Delta/\omega$ is the ratio of the driving intensity and frequency. According to the perturbative expansion ordered by the Bessel functions of the first kind, i.e., $e^{iz\sin y} = \sum_{n=-\infty}^{n=+\infty} J_n(z)e^{iny}$, we have

$$H_I = H_a(e^{i\omega t} + e^{-i\omega t}) + H_0 + \sum_{k=1}^{2}\sum_{n=1}^{\infty}\big[H_n^{(k)}e^{in\omega t}$$
$$+ H_{-n}^{(k)}e^{-in\omega t}\big], \quad (3)$$

where

$$H_a = \frac{g_a}{2}(\sigma^+ a + \sigma^- a^\dagger),$$

$$H_0 = gJ_0(f)\sum_{k=1}^{2}(\sigma^+ m_k + \sigma^- m_k^\dagger),$$

$$H_n^{(k)} = ge^{-if\sin\phi_k}e^{in\phi_k}J_n(f)\sigma^- m_k^\dagger$$
$$+ (-1)^n ge^{if\sin\phi_k}e^{in\phi_k}J_n(f)\sigma^+ m_k, \quad (4)$$

and $H_{-n}^{(k)}$ is the Hermitian conjugate of $H_n^{(k)}$. Using the James method [48,49], the interaction Hamiltonian H_I can therefore be written as

$$H_I \approx H_0 + \frac{1}{\omega}\sum_{k=1}^{2}\big\{[H_a, H_{-1}^{(k)}] + [H_1^{(k)}, H_a]\big\}$$
$$+ \sum_{k=1}^{2}\frac{1}{n\omega}\sum_{n=1}^{\infty}[H_n^{(k)}, H_{-n}^{(3-k)}], \quad (5)$$

up to the order of $O(1/\omega^2)$. The zeroth-order term H_0 describes the effective qubit-magnon interaction under Floquet driving, whose coupling strength $gJ_0(f)$ can be tuned by varying the ratio f. This term is phase independent and can be eliminated by setting $J_0(f) = 0$, i.e., $f \approx 2.4048$. In this situation, we have a σ_z-dependent effective Hamiltonian

$$H_{\text{eff}} = \sigma_z\Big[a^\dagger(g_1 e^{if\sin\phi_1}m_1 + g_2 e^{if\sin\phi_2}m_2)$$
$$- ig_{12}e^{if(\sin\phi_2 - \sin\phi_1)}m_1^\dagger m_2 + \text{H.c.}\Big], \quad (6)$$

where the coupling strengths are

$$g_k = -\frac{g_a g}{\omega}J_1(f)\cos\phi_k, \quad k = 1, 2,$$

$$g_{12} = \frac{2g^2}{\omega}\sum_{n=1}^{\infty}\frac{J_n^2(f)}{n}\sin[n(\phi_2 - \phi_1)]. \quad (7)$$

To render a perfect chiral transfer among the three components a, m_1, and m_2, it is required that $|g_1| = |g_2| = |g_{12}| = g_{\text{eff}}$, i.e., $|\cos(\phi_1)| = |\cos(\phi_2)|$. Note that this condition implies the distinction between driving the coupling strength and driving the frequency in realizing the three-body chirality. In previous works [44,46] for generating a chiral state transfer

by Floquet engineering on the three components' frequencies, the driving phases have to be uniformly distributed in $[0, 2\pi]$, while in our protocol (as a mixture of driving both frequency and coupling strength), the phases ϕ_k are not fixed. A nonunique solution is $\phi_1 = 2\pi/3$ and $\phi_2 = 4\pi/3$, and then

$$g_a = \frac{4g}{J_1(f)} \sum_{n=1}^{\infty} \frac{J_n^2(f)}{n} \sin\left(\frac{2n\pi}{3}\right). \tag{8}$$

Consequently, the effective Hamiltonian in Eq. (6) could be written in a Matrix-product formation,

$$H_{\text{eff}} = \sigma_z [a^\dagger, m_1^\dagger, m_2^\dagger]$$
$$\times g_{\text{eff}} \begin{bmatrix} 0 & e^{\frac{i\sqrt{3}f}{2}} & e^{-\frac{i\sqrt{3}f}{2}} \\ e^{-\frac{i\sqrt{3}f}{2}} & 0 & -ie^{-i\sqrt{3}f} \\ e^{\frac{i\sqrt{3}f}{2}} & ie^{i\sqrt{3}f} & 0 \end{bmatrix} \begin{bmatrix} a \\ m_1 \\ m_2 \end{bmatrix}, \tag{9}$$

which is convenient to obtain the time evolution of the continuous-variable operators

$$\begin{bmatrix} a(t) \\ m_1(t) \\ m_2(t) \end{bmatrix} = \hat{T}(t) \begin{bmatrix} a(0) \\ m_1(0) \\ m_2(0) \end{bmatrix}. \tag{10}$$

Here, $\hat{T}(t)$ depends on the qubit state. When the qubit is in the excited state $|e\rangle$, we have

$$\hat{T}(t) = \hat{T}^{(e)}(t)$$
$$= \frac{1}{3} \begin{bmatrix} x(t) & -ie^{\frac{i\sqrt{3}f}{2}}y(t) & ie^{-\frac{i\sqrt{3}f}{2}}z(t) \\ ie^{-\frac{i\sqrt{3}f}{2}}z(t) & x(t) & -e^{-i\sqrt{3}f}y(t) \\ -ie^{\frac{i\sqrt{3}f}{2}}y(t) & -e^{i\sqrt{3}f}z(t) & x(t) \end{bmatrix}, \tag{11}$$

where

$$x(t) = 1 + 2\cos(\sqrt{3}g_{\text{eff}}t),$$
$$y(t) = 1 + 2\cos\left(\sqrt{3}g_{\text{eff}}t - \frac{2\pi}{3}\right),$$
$$z(t) = 1 + 2\cos\left(\sqrt{3}g_{\text{eff}}t + \frac{2\pi}{3}\right). \tag{12}$$

The transformation matrix $\hat{T}^{(e)}$ entails a sufficient condition for a clockwise and periodic chirality. It is interesting to find that $m_2(t) = a(0)$, $m_1(t) = m_2(0)$, and $a(t) = m_1(0)$ when $t = (2\pi/3 + 2n\pi)/(\sqrt{3}g_{\text{eff}})$; $m_2(t) = m_1(0)$, $m_1(t) = a(0)$, and $a(t) = m_2(0)$ when $t = (4\pi/3 + 2n\pi)/(\sqrt{3}g_{\text{eff}})$; and $m_k(t) = m_k(0)$, $a(t) = a(0)$ when $t = 2n\pi/(\sqrt{3}g_{\text{eff}})$ with n integer. This transfer is exactly the rotation $a \rightarrow m_2 \rightarrow m_1 \rightarrow a$ described by the straight-line arrows in Fig. 1, corresponding to a clockwise chiral propagation of states in the Schrödinger picture, i.e., $|\varphi_a \varphi_1 \varphi_2\rangle \rightarrow |\varphi_1 \varphi_2 \varphi_a\rangle \rightarrow |\varphi_2 \varphi_1 \varphi_a\rangle$, where $|\varphi_a\rangle$ and $|\varphi_k\rangle$ are arbitrary states for the resonator and magnonic mode k, respectively.

Suppose that the resonator is prepared as an arbitrary superposed state $C_n |n\rangle$ and the two magnonic modes are in their ground states, i.e.,

$$|\varphi(0)\rangle = \sum_n C_n |n00\rangle = \sum_n \frac{C_n}{\sqrt{n!}}(a^\dagger)^n |000\rangle. \tag{13}$$

By virtue of Eq. (11), it is straightforward to express the time-evolved state as

$$|\varphi(t)\rangle = \sum_n \frac{C_n}{\sqrt{n!}}\big[a^\dagger \hat{T}_{11}^{(e)\dagger}(t) + m_1^\dagger \hat{T}_{12}^{(e)\dagger}(t)$$
$$+ m_2^\dagger \hat{T}_{13}^{(e)\dagger}(t)\big]^n |000\rangle. \tag{14}$$

For example, when $|\varphi(0)\rangle = |100\rangle$, we have

$$|\varphi(t)\rangle = \frac{1}{3}[x(t)|100\rangle - ie^{\frac{i\sqrt{3}f}{2}}z(t)|010\rangle$$
$$+ ie^{\frac{-i\sqrt{3}f}{2}}y(t)|001\rangle]. \tag{15}$$

We can have a unit transfer fidelity at the desired moments for the general superposed state in Eq. (13), e.g., when $t = 2\pi/(3\sqrt{3}g_{\text{eff}})$, $|\varphi(t)\rangle = \sum_n C_n |00n\rangle$. To avoid the influence from local phases [56] during the whole evolution, the state-transfer fidelity can be measured by time-dependent state populations

$$P_j(t) = \sum_{C_n \neq 0} |\langle \varphi(t)|n\rangle_j|^2, \tag{16}$$

where $|n\rangle_j$, $j = a, 1, 2$, indicates that the marked mode is in the Fock state $|n\rangle$ and the other two modes are in their ground states.

In parallel to Eq. (11), we have

$$\hat{T}(t) = \hat{T}^{(g)}(t)$$
$$= \frac{1}{3} \begin{bmatrix} x(t) & -ie^{\frac{i\sqrt{3}f}{2}}z(t) & ie^{-\frac{i\sqrt{3}f}{2}}y(t) \\ ie^{-\frac{i\sqrt{3}f}{2}}y(t) & x(t) & -e^{-i\sqrt{3}f}z(t) \\ -ie^{\frac{i\sqrt{3}f}{2}}z(t) & -e^{i\sqrt{3}f}y(t) & x(t) \end{bmatrix}, \tag{17}$$

when the qubit is in the ground state $|g\rangle$. The transformation matrix $\hat{T}^{(g)}$ indicates an anticlockwise chirality, yielding the transfer along the rotation $a \rightarrow m_1 \rightarrow m_2 \rightarrow a$ described by the curved arrows in Fig. 1. Then, in the Schrödinger picture, a chiral evolution emerges as $|\varphi_a \varphi_1 \varphi_2\rangle \rightarrow |\varphi_2 \varphi_a \varphi_1\rangle \rightarrow |\varphi_1 \varphi_2 \varphi_a\rangle$. For the same initial states in Eq. (13), we have

$$|\varphi(t)\rangle = \sum_n \frac{C_n}{\sqrt{n!}}\big[a^\dagger \hat{T}_{11}^{(g)\dagger}(t) + m_1^\dagger \hat{T}_{12}^{(g)\dagger}(t)$$
$$+ m_2^\dagger \hat{T}_{13}^{(g)\dagger}(t)\big]^n |000\rangle \tag{18}$$

by virtue of Eq. (17).

Figures 2(a) and 2(b) show the time-evolved state populations $P_j(t)$ under the effective Hamiltonian (6) (see the lines with markers) and the system Hamiltonian in Eq. (1) (see the lines with no markers), demonstrating, respectively, the clockwise and anticlockwise chirality. The numerical and analytical results are found to match perfectly with each other. The qubit state determines the chiral direction. A superposed state of the qubit gives rise to two chiral directions, which are demanded to generate the NOON state. The period of the chiral state propagation is state independent and uniquely determined by the coupling strengths in Eq. (7) under the condition $J_0(f) = 0$.
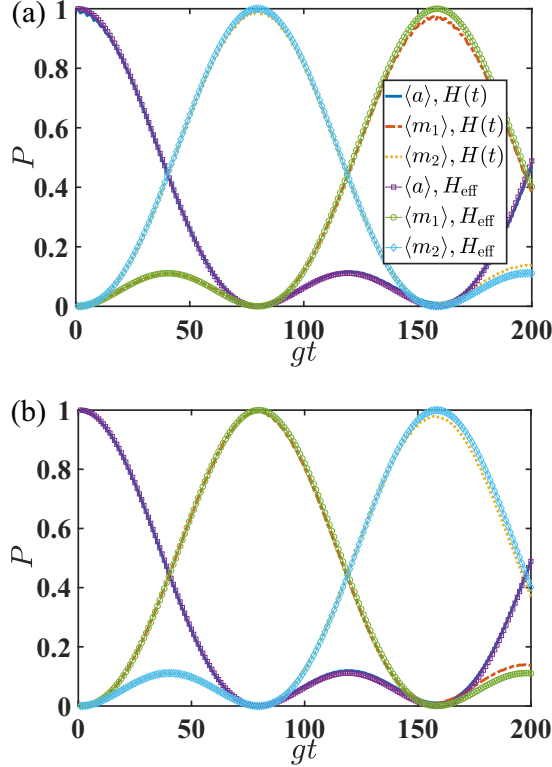
(a)

(b)

FIG. 2. Chiral dynamics of the state populations P_j for the three modes, $j = a, 1, 2$, by numerical simulation with the Floquet engineering Hamiltonian (1) and analytical evaluation with the effective Hamiltonian (6). In (a), the qubit is at $|e\rangle$ and in (b), it is at $|g\rangle$. The three modes are initialized as $|1\rangle_a|0\rangle_{m_1}|0\rangle_{m_2}$. The parameters are set as $\omega = 20g$, $f = \Delta/\omega = 2.4048$, $\phi_1 = 2\pi/3$, and $\phi_2 = 4\pi/3$.

III. SYSTEMATIC ERRORS

In practice, the ideal chiral state transfer in Fig. 2 using the effective Hamiltonian (6) cannot be exactly realized because of the imperfections and constraints in experiments. Even under the desired conditions in the last section, i.e., fast engineering, exact cancellation of the phase-independent term, and accurate setting of the coupling strength, it is inevitable to estimate the perturbative effect on the transport protocols from the fluctuations in parameters of the full Hamiltonian. In the rest of this section, we analyze the systematic errors induced by the qubit-magnon coupling-strength deviation, the unstable Floquet driving, the mismatch of the magnon frequencies, and the presence of the counterrotating interactions.

A. The qubit-magnon coupling-strength deviation

The coupling strengths between qubit and magnonic modes [the last term in Eq. (1)] are chosen the same in magnitude. They depend practically on the distance between the YIG spheres and the qubit. We first consider their deviation from a fixed value. The system Hamiltonian can thus be rewritten as

$$
\begin{aligned}
H' = {} & g_a \cos(\omega t)(\sigma^+ a + \sigma^- a^\dagger) \\
& + \Delta \cos(\omega t + \phi_1) m_1^\dagger m_1 + g(1+\delta)(\sigma^+ m_1 + \sigma^- m_1^\dagger) \\
& + \Delta \cos(\omega t + \phi_2) m_2^\dagger m_2 + g(1-\delta)(\sigma^+ m_2 + \sigma^- m_2^\dagger),
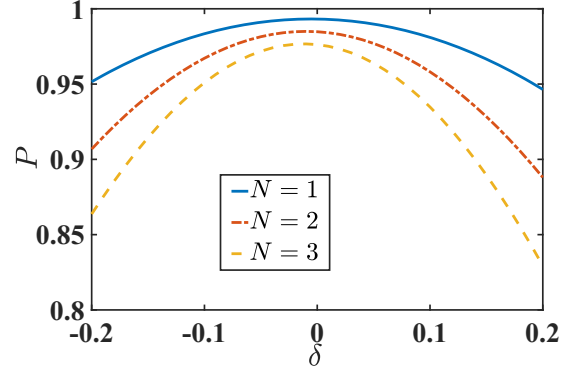\end{aligned}
\tag{19}
$$

FIG. 3. Chiral state-transfer fidelity of the target state $(|e00N\rangle + |g0N0\rangle)/\sqrt{2}$ under the nonideal Hamiltonian (19) as a function of the systematic error associated with the qubit-magnon coupling strength. Ideally (under the effective Hamiltonian) the initial state $(|eN00\rangle + |gN00\rangle)/\sqrt{2}$ would become the target state at the desired moment $T = 2\pi/(3\sqrt{3}g_{\text{eff}})$. Here the parameters are set the same as Fig. 2.

where δ represents the magnitude of the relative error. Under the same settings that $\phi_1 = 2\pi/3$, $\phi_2 = 4\pi/3$, $J_0(f = \Delta/\omega) = 0$, and $|g_k| = |g_{12}|$ in Eq. (7) for the chiral transfer, the effective Hamiltonian in Eq. (9) is modified by changing the coefficient matrix into

$$
g_{\text{eff}}
\begin{bmatrix}
0 & (1+\delta)e^{\frac{i\sqrt{3}f}{2}} & (1-\delta)e^{-\frac{i\sqrt{3}f}{2}} \\
(1+\delta)e^{-\frac{i\sqrt{3}f}{2}} & 0 & -i(1-\delta^2)e^{-i\sqrt{3}f} \\
(1-\delta)e^{\frac{i\sqrt{3}f}{2}} & i(1-\delta^2)e^{i\sqrt{3}f} & 0
\end{bmatrix}.
\tag{20}
$$

It can be perturbatively decomposed into

$$
H'_{\text{eff}} = H_{\text{eff}} + \delta H_1 + \delta^2 H_2,
\tag{21}
$$

where H_{eff} is the unperturbed effective Hamiltonian in Eq. (9). H_1 is the leading-order perturbation, whose coefficient matrix reads

$$
g_{\text{eff}}
\begin{bmatrix}
0 & e^{\frac{i\sqrt{3}f}{2}} & -e^{-\frac{i\sqrt{3}f}{2}} \\
e^{-\frac{i\sqrt{3}f}{2}} & 0 & 0 \\
-e^{\frac{i\sqrt{3}f}{2}} & 0 & 0
\end{bmatrix}.
\tag{22}
$$

Using the method in Ref. [57] and up to the second order of the systematic error δ, one can obtain the population p of the magnon mode m_2 for the transfer $|e100\rangle \rightarrow |e001\rangle$ at the desired time $T = 2\pi/(3\sqrt{3}g_{\text{eff}})$ as

$$
p = 1 - \sum_{j=1}^{2} \left| \int_0^T dt \langle 0|m_j(t)|\delta H_1|a^\dagger(t)|0\rangle \right|^2 = 1 - \delta^2,
\tag{23}
$$

where $a(t)$ and $m_j(t)$ are the time-evolved operators given in Eq. (10) and $|0\rangle \equiv |0\rangle_a|0\rangle_{m_1}|0\rangle_{m_2}$ is the vacuum state. By the population definition in Eq. (16), the state-transfer population P for $|e00N\rangle$ from $|eN00\rangle$ can then be estimated as $P = p^N = (1 - \delta^2)^N \approx 1 - N\delta^2$. This result applies also to the state transfer $|gN00\rangle \rightarrow |g00N\rangle$. The nonideal dynamics under Hamiltonian (19) are provided in Fig. 3 by the sensitivity of the transfer fidelity (population) of the target state $|\Phi(t)\rangle = (|e00N\rangle + |g0N0\rangle)/\sqrt{2}$ that evolves from the initial

TABLE I. Chiral state-transfer population of the target state $(|e00N\rangle + |g0N0\rangle)/\sqrt{2}$ under the total Hamiltonian in Eq. (19) with $\delta = 0$. Here the parameters are set the same as Fig. 2.

N	1	2	3	4	5	6	7	8	9	10
P	0.98	0.97	0.95	0.93	0.90	0.87	0.84	0.80	0.76	0.72

state $|\Phi(0)\rangle = (|eN00\rangle + |gN00\rangle)/\sqrt{2}$, to δ. The populations are evaluated at T, which is determined by the ideal chiral state transfers depending on Eqs. (11) and (17). The state-transfer population in general declines with increasing $|\delta|$ and N. Our protocol is found to be robust even under $|\delta| \approx 20\%$ and $N = 3$, whereby the population is about 0.85.

Note that H_{eff} is the second-order perturbation over H, so that one can find a less-than-unit population even when $\delta = 0$. We list the results for various N in Table I. The transfer population decreases monotonically with N and it becomes less than 0.80 when $N > 8$. It is due to the fact that the second-order effective Hamiltonian is applicable in the regime $g \ll \omega$ and g becomes practically $g\sqrt{N}$ for $|N\rangle$.

B. The unstable Floquet driving

To cancel the phase-independent term from the interaction Hamiltonian (5) for a chiral propagation of quantum states, the ratio $f = \Delta/\omega$ of the Floquet-driving intensity Δ and the frequency ω is fixed to meet the requirement $J_0(f) = 0$. We now estimate the effect of the control error arising from the Floquet-driving intensity, which is unstable in the time domain. The error could then be regarded as random fluctuations. The Hamiltonian in Eq. (1) can thus be modified to

$$H' = g_a \cos(\omega t)(\sigma^+ a + \sigma^- a^\dagger)$$
$$+ \Delta \sum_{k=1}^{2}(1 + \epsilon_k)\cos(\omega t + \phi_k)m_k^\dagger m_k$$
$$+ g \sum_{k=1}^{2}(\sigma^+ m_k + \sigma^- m_k^\dagger), \quad (24)$$

where ϵ_k indicates a dimensionless factor for the driving intensity on the magnonic mode k. It is assumed to be a random number in the range of $[0, \epsilon]$ with $\epsilon < 1$ and $\epsilon_1 \neq \epsilon_2$.

In Fig. 4, we present the sensitivity of the state-transfer population to the error upper bound ϵ. The initial state is chosen as $|\Phi(0)\rangle = (|e200\rangle + |g200\rangle)/\sqrt{2}$ and then the target state is $|\Phi[T = 2\pi/(3\sqrt{3}g_{\mathrm{eff}})]\rangle = (|e002\rangle + |g020\rangle)/\sqrt{2}$. The populations, measured by the maximum P_{max}, the minimum P_{min}, and the average values $\bar{P}$, are obtained by 100 numerical simulations using randomly distributed ϵ_k's. The distance between P_{max} and P_{min} is found to decrease roughly with increasing ϵ. The average population $\bar{P}$ can be maintained above 0.90 when $\epsilon \leqslant 0.1$, and above 0.70 when $\epsilon \leqslant 0.2$. However, the minimum value P_{min} declines to below 0.50 when ϵ approaches 0.1. It implies a dramatic error caused by the fluctuation in the Floquet driving intensity, which is more significant than that in the qubit-magnon coupling strength.
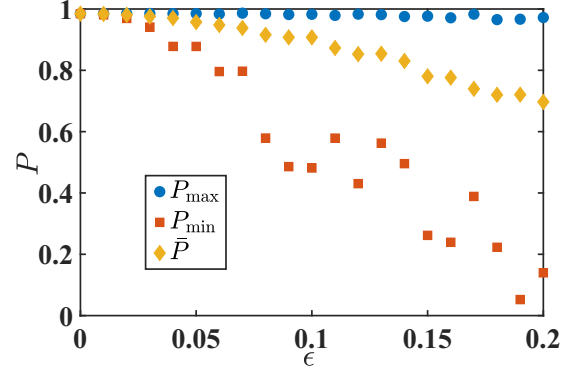

FIG. 4. Chiral state-transfer fidelity of the target state $(|e002\rangle + |g020\rangle)/\sqrt{2}$ under the nonideal Hamiltonian (24) as a function of the systematic error associated with the Floquet-driving intensity. The circles, squares, and diamonds represent the maximum P_{max}, minimum P_{min}, and average populations $\bar{P}$, respectively. Here the parameters are set the same as Fig. 2.

For a constant deviation $\epsilon_1 = \epsilon_2 = \epsilon$, we have an extra term in addition to the ideal effective Hamiltonian in Eq. (6), i.e.,

$$H'_{\mathrm{eff}} = H_0 + H_{\mathrm{eff}}, \quad (25)$$

where H_0 is the zeroth-order term in Eq. (4) and the ratio f in both H_0 and H_{eff} is replaced with $f' = f(1 + \epsilon)$. When $\epsilon = 0.005$, the chiral state-transfer fidelity is found to be $P = 0.84$ under H'_{eff} in Eq. (25), and it is about $P = 0.82$ under the full Hamiltonian in Eq. (24). When $\epsilon = 0.01$, it drops to $P = 0.50$ and $P = 0.49$, respectively. Thus, the fidelity is sensitive to the error arisen from the unstable Floquet driving intensity. To render a perfect chiral state transfer among components a, m_1, and m_2, the magnitude of the zeroth order should be kept as low as possible, i.e., $gJ_0(f') \ll g_{\mathrm{eff}}$.

C. The frequency mismatch of magnons and qubit

The four components in our system, i.e., the superconducting qubit, the resonator, and two magnonic modes, are supposed to be resonant with each other in the microwave regime in Sec. II. It is challenging to achieve such accurate resonance in experiments. Therefore, the frequency mismatch effects on chiral state-transfer fidelity are important.

For the frequency mismatch of the two magnon modes, the deviated Hamiltonian in the Schrödinger picture could be written as

$$H' = \omega_a(a^\dagger a + \sigma^+ \sigma^-) + \omega_a \sum_{k=1}^{2}(1 + \chi_k)m_k^\dagger m_k + H, \quad (26)$$

where $\chi_1 = \chi$, $\chi_2 = -\chi$, χ represents the relative magnitude of the frequency mismatch, and H is the Hamiltonian in Eq. (1). In Fig. 5(a), the chiral state transfer population dynamics from the initial state $|\Phi(0)\rangle = (|e200\rangle + |g200\rangle)/\sqrt{2}$ is presented under various χ. One can observe that the population dynamics when $\chi = 10^{-5}$ is close to the dynamics free of mismatch. And the target state population can be maintained above 0.95. It is reduced to 0.4 when $\chi = 10^{-4}$. Nevertheless, our protocol is promising in the recent experiments [58] since
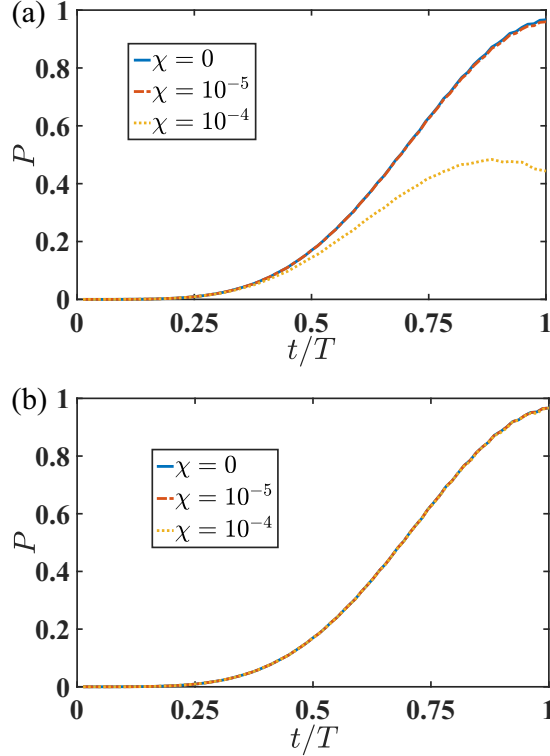
FIG. 5. [(a) and (b)]: Chiral state-transfer population of the target state $(|e002\rangle + |g020\rangle)/\sqrt{2}$ under the deviated system Hamiltonians (26) and (27) with various error magnitude χ, which are associated with the magnons and qubit frequency mismatch, respectively. Here the parameters are set the same as Fig. 2 and $T = 2\pi/(3\sqrt{3}g_{\rm eff})$.

the bandwidths of the resonator and magnon modes are found to be around $10^{-6} \sim 10^{-5}\omega_a$.

For the frequency deviation from the qubit, the Hamiltonian turns out to be

$$H' = \omega_a a^\dagger a + \omega_a(1+\chi)\sigma^+\sigma^- + \omega_a\sum_{k=1}^{2}m_k^\dagger m_k + H. \quad (27)$$

One can find in Fig. 5(b) that this deviation has no significant effect on the state transfer dynamics, as the three lines under various χ are almost the same. It can be understood by the effective Hamiltonian, which is found to be $H'_{\rm eff} = \chi\omega_a\sigma^+\sigma^- + H_{\rm eff}$. The extra term about the qubit-frequency mismatch is clearly irrelevant to the chiral state transfer dynamics among the other three bosonic modes.

D. The presence of the counterrotating interaction

Back to the laboratory frame, the full Hamiltonian under the resonant condition without the rotating-wave approximation is written as

$$H' = \omega_a(a^\dagger a + \sigma^+\sigma^-)$$

$$+ \sum_{k=1}^{2}[\omega_a + \Delta\cos(\omega t + \phi_k)]m_k^\dagger m_k$$

$$+ g_a\cos(\omega t)(\sigma^+ a + \sigma^- a^\dagger + \sigma^+ a^\dagger + \sigma^- a)$$

$$+ \sum_{k=1}^{2}g(\sigma^+ m_k + \sigma^- m_k^\dagger + \sigma^+ m_k^\dagger + \sigma^- m_k), \quad (28)$$

where ω_a represents the characteristic frequency of the four components. In the Hamiltonian H (1) used for our chiral state-transfer protocol, both qubit-resonator and qubit-magnon coupling strengths g_a and g have to be much smaller than the transition frequency ω_a in magnitude. Although a faster speed of the chiral transfer favors a larger g_a or g, a constraint for their magnitude has to be estimated by including the counterrotating interactions into the original Hamiltonian H'.

Using the James method [48,49], the ideal effective Hamiltonian in Eq. (6) becomes

$$H'_{\rm eff} = \sigma_z\left[a^\dagger\sum_{k=1}^{2}g'_k e^{if\sin\phi_k}m_k\right.$$

$$\left. -ig'_{12}e^{if(\sin\phi_2 - \sin\phi_1)}m_1^\dagger m_2 + {\rm H.c.}\right],$$

$$+ \sigma_z\delta(2\omega_a - n'\omega)\left[a^\dagger\sum_{k=1}^{2}G'_k e^{-if\sin\phi_k}m_k^\dagger\right.$$

$$\left. + G'_{12}e^{-if(\sin\phi_2 + \sin\phi_1)}m_1^\dagger m_2^\dagger + {\rm H.c.}\right] \quad (29)$$

with

$$g'_k = -g_a g J_1(f)\cos\phi_k\left(\frac{1}{\omega} - \frac{1}{2\omega_a + \omega}\right), \quad k = 1, 2,$$

$$g'_{12} = 2g^2\sum_{n=1}^{\infty}\left(\frac{1}{n\omega} - \frac{1}{2\omega_a + n\omega}\right)J_n^2(f)\sin[n(\phi_2 - \phi_1)],$$

$$G'_k = (-1)^{n'-1}\frac{g_a g}{\omega}\left[\frac{n'e^{-i(n'-1)\phi_k}J_{n'-1}(f)}{n'-1}\right.$$

$$\left. -\frac{n'e^{-i(n'+1)\phi_k}J_{n'+1}(f)}{n'+1}\right],$$

$$G'_{12} = \frac{g^2}{\omega}\sum_{n=1}^{\infty}(-1)^{n+n'}\frac{n'}{n(n'+n)}J_n(f)J_{n+n'}(f)$$

$$\times\{e^{-i[n\phi_1 - (n+n')\phi_2]} + e^{-i[n\phi_2 - (n+n')\phi_1]}\}$$

$$+ \frac{g^2}{\omega}(-1)^{n'}\sum_{n=1}^{n'-1}\frac{1}{n}J_n(f)J_{n'-n}(f)$$

$$\times[e^{in\phi_1 + i(n'-n)\phi_2} + e^{in\phi_2 + i(n'-n)\phi_1}]. \quad (30)$$

The counterrotating interactions ($a^\dagger m_1^\dagger$, $a^\dagger m_2^\dagger$, and $m_1^\dagger m_2^\dagger$) could be omitted when $\omega_a \gg \omega$ (even when $2\omega_a \approx n'\omega$). In this case, the effective coupling strengths $g'_k \approx g_k \gg G'_k$, $g'_{12} \approx g_{12} \gg G'_{12}$, and $J_{n'-1}(f) \ll J_1(f)$, $J_n(f)J_{n+n'}(f) \ll J_n^2(f)$ and $J_n(f)J_{n'-n}(f) \ll J_n^2(f)$ for $f = 2.4048$ and $n' \gg 1$. On the other hand, the perturbative method based on the James effective Hamiltonian is valid when the Floquet-driving frequency $\omega \gg g$. Thus, the Floquet driving frequency in our
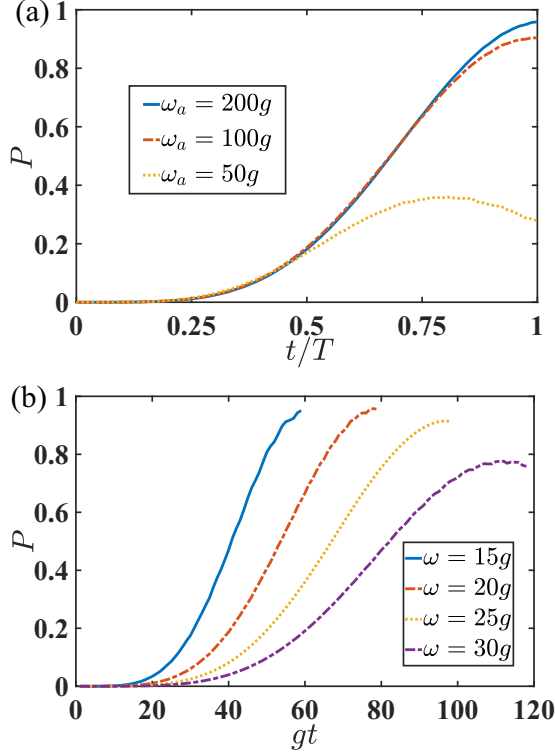
FIG. 6. Chiral state-transfer fidelity of the target state $(|e002\rangle + |g020\rangle)/\sqrt{2}$ under the system Hamiltonian (28) holding the counter-rotating interactions with (a) varying transition frequency ω_a and a fixed $\omega = 20g$, and (b) varying Floquet driving frequency ω and a fixed $\omega_a = 200g$. Note that the evolution period $T = 2\pi/(3\sqrt{3}g_{\rm eff})$ is independent of ω_a but dependent on ω. The other parameters are set the same as Fig. 2.

protocol should be in a compromise regime, given transition frequency ω_a and coupling strength g.

Figure 6(a) is used to reveal the implicitly required magnitude of ω_a to justify the system Hamiltonian H in our protocol. We demonstrate the effect of the counterrotating interactions by the chiral state-transfer population dynamics from the initial state $|\Phi(0)\rangle = (|e200\rangle + |g200\rangle)/\sqrt{2}$ under varying transition frequency ω_a. It is found that the population can be maintained above 0.90 when $\omega_a = 100g$ and above 0.98 when $\omega_a = 200g$. A smaller ω_a yields a lower P. When ω_a decreases to $\omega_a = 50g$, P is lower than 0.30 in the end of the evolution. In Fig. 6(b), we plot the chiral state-transfer population dynamics for the same state under varying transition frequency ω. It is found that the population can be maintained above 0.90 in the regime of $15 < \omega/g < 25$. However, when $\omega = 30g$, P is lower than 0.75 in the end of the evolution with $T = 2\pi/(3\sqrt{3}g_{\rm eff})$. Thus, our protocol is not appropriate in the strong Floquet regime.

IV. NOON STATE GENERATION AND FIDELITY ANALYSIS

This section provides the details of generating the magnonic NOON states based on the Floquet-engineering Hamiltonian (1) under the qubit-dependent chiral-transfer
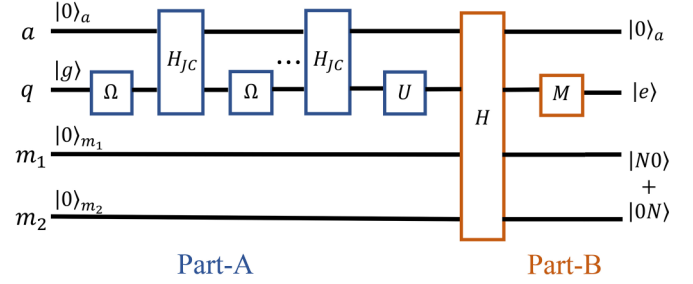

FIG. 7. Circuit model of the magnonic NOON state generation. Part A is used to prepare the resonator as a Fock state $|N\rangle$ and the qubit as a symmetrical-superposed state. It consists of a sequence of π pulses on qubit characterized by the Rabi frequency Ω, the local evolution of qubit and resonator under a Jaynes-Cummings Hamiltonian $H_{\rm JC}$ (31), and a final $\pi/2$ pulse U (34) on qubit. In Part B, after the global evolution under the Floquet-engineering Hamiltonian (1), a bare-basis projection is performed on qubit to yield the magnonic NOON state.

condition. Also, we analyze the protocol fidelity in the presence of the quantum dissipation.

A. Preparing NOON state with multiple excitations

Suppose that all four components in our hybrid system (qubit, resonator mode, and two magnonic modes) are initially in their ground states, i.e., $|\Phi(0)\rangle = |g000\rangle = |g\rangle_q|0\rangle_a|0\rangle_{m_1}|0\rangle_{m_2}$. The generation procedure of a magnonic NOON state could be constituted by two parts, A and B.

As illustrated by the circuit model in Fig. 7, Part A is mainly used to prepare the resonator mode as an arbitrary Fock state $|N\rangle$. Accordingly, it is divided into $N + 1$ steps as follows. This part is local to the resonator and the qubit. Then, to avoid unnecessary crosstalk with the two magnons, the resonator and the qubit are detuned to be far-off-resonant from them. Also, we temporally remove the time modulation over the coupling strength between qubit and resonator. Thus, in Part A we have a Jaynes-Cummings Hamiltonian

$$H_{\rm JC} = g_a(\sigma^+ a + \sigma^- a^\dagger). \tag{31}$$

Step A_1. A microwave π pulse of $\{\omega_q, \pi/(2\Omega)\}$ is applied to the qubit and the system state is transformed to be $|\Phi(\tau)\rangle = |e000\rangle$ up to a global phase. Here, ω_q is the pulse frequency, which is currently resonant with the qubit. $\tau \equiv \pi/(2\Omega)$ is the duration time of the pulse. The Rabi frequency Ω is assumed to be much larger than g_a to make it reasonable to ignore the evolution under $H_{\rm JC}$ during a sufficiently short period τ. Then, turning on the Hamiltonian (31) for a period of $\tau_1 = \pi/(2g_a)$, we have

$$|\Phi(\tau + \tau_1)\rangle = -|g100\rangle. \tag{32}$$

Step A_j, $j = 2, \ldots, N$. We alternatively employ the same microwave π pulse $\{\omega_q, \pi/(2\Omega)\}$ to pump the qubit from the ground state to the excited state and switch on and off the Hamiltonian (31) with a decreasing duration time $\tau_j = \pi/(2\sqrt{j}g_a)$ to transform $|e(j-1)00\rangle$ to be $|gj00\rangle$. Therefore, after these steps, the system state becomes

$$|\Phi(T_A)\rangle = (-1)^N|gN00\rangle, \tag{33}$$

where $T_A = N\tau + \sum_{j=1}^{N} \tau_j$. Till now, a number state is created in the resonator mode. The global phase $(-1)^N$ can be ignored for simplicity.

Step A_{N+1}. A $\pi/2$-pulse gate is performed on a qubit. It can be expressed by

$$U = e^{i(\pi/4)\vec{\sigma}\cdot\vec{n}} = \frac{1}{\sqrt{2}}\begin{bmatrix} 1 & ie^{-i\theta} \\ ie^{i\theta} & 1 \end{bmatrix}, \qquad (34)$$

where $\vec{\sigma} \equiv (\sigma_x, \sigma_y, \sigma_z)$ and $\vec{n} = (\cos\theta, \sin\theta, 0)$. The qubit becomes a superposed state and the system state reads

$$|\Phi(T_A)\rangle = \frac{1}{\sqrt{2}}(|g\rangle + ie^{i\theta}|e\rangle)|N00\rangle, \qquad (35)$$

where the phase θ is tunable as desired and can be regarded as an encoded local phase for the NOON state.

In the beginning of Part *B*, we are well prepared to generate the magnonic NOON state based on the full Hamiltonian (1) and the system state in Eq. (35). Here, the qubit is in charge of controlling the direction of the chiral state transfer to make the Fock state $|N\rangle$ of the resonator to be perfectly transferred to the two magnonic modes at the same time.

Step B_1. Under the desired time modulations over the qubit-resonator interaction and the Floquet engineering over the magnonic modes to achieve the effective Hamiltonian in Eq. (6), the system state evolves to

$$|\Phi(T_A + T)\rangle = \frac{1}{\sqrt{2}}(|g0N0\rangle - ie^{i\theta}|e00N\rangle) \qquad (36)$$

after $T = 2\pi/(3\sqrt{3}g_{\text{eff}})$, according to the transformation matrices in Eqs. (11) and (17). Then, we detune the qubit frequency and apply a microwave $\pi/2$ pulse $\{\omega_q, \pi/(4\Omega)\}$ to the qubit. The state becomes

$$|\Phi(T_B = T_A + T + \tau/2)\rangle$$
$$= \frac{1}{2}(|g0N0\rangle - e^{i\theta}|g00N\rangle) - \frac{i}{2}(|e0N0\rangle + e^{i\theta}|e00N\rangle)$$
$$= \frac{1}{2}|g0\rangle(|N0\rangle - e^{i\theta}|0N\rangle) - \frac{i}{2}|e0\rangle(|N0\rangle + e^{i\theta}|0N\rangle). \qquad (37)$$

Step B_2. In the final step, one can obtain the magnonic NOON state $(|N0\rangle - e^{i\theta}|0N\rangle)/\sqrt{2}$ or $(|N0\rangle + e^{i\theta}|0N\rangle)/\sqrt{2}$ by performing a projective measurement on the ground or the excited state of the qubit. To hold the NOON state, the frequencies of all four components can then be offset to avoid unnecessary evolution. With a typical coupling strength between the qubit and magnon $g/2\pi \sim 20$ MHz [38], it is found that $T_B \approx 0.65\,\mu s$ for $N = 5$ when the tuning time is omitted (e.g., the pulse duration is nearly 10 ns [59]). So, the full generation time is much smaller than the relaxation time of magnon of about 10 μs [25].

In a general situation where the resonator is initialed as an arbitrary state $|\varphi\rangle$ and the two magnons are in the same state $|\beta\rangle$, one can generate a (nonnormalized) entangled state $|\varphi\rangle|\beta\rangle + |\beta\rangle|\varphi\rangle$ of the two magnonic modes through Part *B*. For example, if $|\varphi\rangle$ is a coherent state $|\alpha\rangle$ and $|\beta\rangle = |0\rangle$, then the final state of two magnonic modes would be a (nonnormalized) cat state [60] $|\alpha\rangle|0\rangle + |0\rangle|\alpha\rangle$ as long as the qubit is prepared as the superposed state in Eq. (35). The state of the
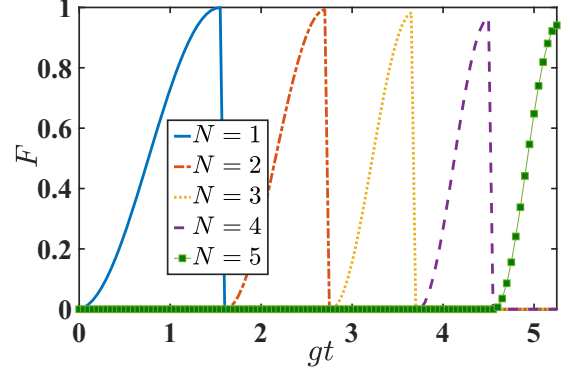

FIG. 8. Fidelity during the process of generating Fock-state $|N = 5\rangle$ of the resonator mode a as indicated in Eq. (33). All the lines except the green solid line marked with squares indicate the intermediate result about the overlap between evolved state and $|N < 5\rangle$. $\Omega = 30g$, $g_a = g$, and $\gamma/g = 10^{-5}$.

magnons could be detected in experiments by the integrated superconducting qubit and nitrogen vacancy center [25,32].

B. Fidelity analysis

The physical feasibility of our generation protocol could be verified by the numerical simulation over the whole procedure in Sec. IV A. The overlap of the final state and the ideal NOON state at the end of Step B_2 could be regarded as the generation-protocol fidelity. In particular, we prepare the whole system as a product of ground state, follow all the steps in Parts *A* and *B*, and take into account the decoherence from all components of the hybrid system into the dynamics. Under the standard Markovian approximation and tracing out the degrees of freedom of the external environment (assumed to be at the vacuum state), we arrive at the master equation for the density-matrix operator $\rho(t)$ of the whole system consisting of qubit, resonator, and magnonic modes:

$$\dot{\rho}(t) = -i[\tilde{H}, \rho(t)] + \kappa_a \mathcal{L}[a]\rho(t) + \kappa_m \mathcal{L}[m_1]\rho(t)$$
$$+ \kappa_m \mathcal{L}[m_2]\rho(t) + \gamma \mathcal{L}[\sigma^-]\rho(t). \qquad (38)$$

In Part *A* for the local evolution of qubit and resonator, $\tilde{H} = H_{\text{JC}}$ (31), and in Part *B* for the global evolution, $\tilde{H} = H$ (1). κ_a, κ_m, and γ are the decoherence rates of the resonator, the magnonic modes, and the qubit, respectively. To simplify the discussion but with no loss of generality, we set $\kappa_a = \kappa_m = \gamma$. These rates are surely dependent on the magnitude of the associated transitions in spontaneous emission. Yet this setting is simply used to estimate the robustness of the ideal protocol, so all of the decoherence rates are supposed to be in the same order of magnitude. The dissipative superoperator $\mathcal{L}$ is defined in a Lindblad form,

$$\mathcal{L}[o]\rho \equiv \frac{1}{2}(2o\rho o^\dagger - o^\dagger o\rho - \rho o^\dagger o), \qquad (39)$$

where $o = \sigma^-, a, m_1, m_2$ are the decay operators.

Before taking the crucial steps of generating a NOON state by chiral state transfer, as discussed in Sec. II, we have to consider the nonideal dynamics during Part *A* to achieve a desired Fock state of the resonator. In Fig. 8, the fidelity dynamics of $|N = 5\rangle$ is plotted by using the master
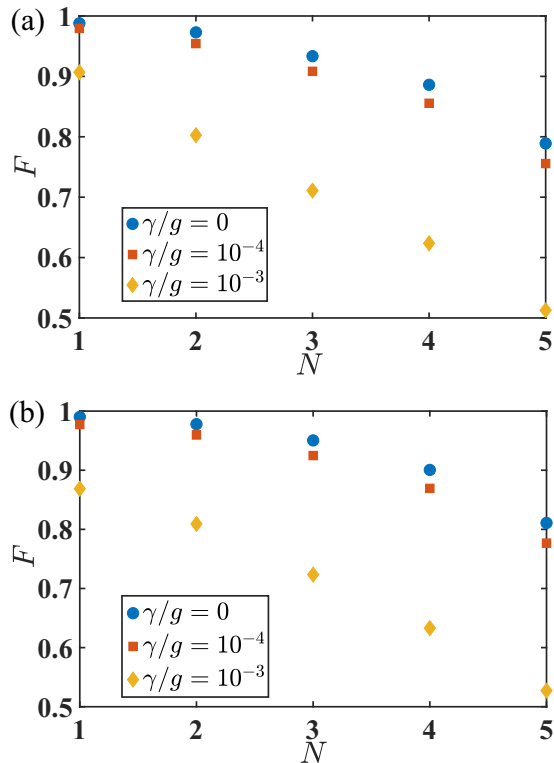
FIG. 9. Fidelity of the NOON state obtained by the projective measurement over (a) the excited state and (b) the ground state of the qubit (see Step B_2 in Sec. IV A), under varying decoherence rate γ. Here the parameters are set as $\omega = 20g$, $\phi_1 = 2\pi/3$, $\phi_2 = 4\pi/3$, $\theta = \pi$, and $\Omega = 30g$.

equation (38). On this stage, the magnons are separable. The five peak values indicate the temporal fidelity of $|N \leqslant 5\rangle$ during the step-by-step process, which decline with N. In particular, we have $F = 0.95$ for $N = 5$.

Using Eq. (37), Step B_2, and Eq. (38), the final fidelity is calculated by $F = \langle\Psi|\mathrm{Tr}_{qr}[\rho(T_B)]|\Psi\rangle$, where $|\Psi\rangle$ is the target magnonic NOON state and $\mathrm{Tr}_{qr}[\cdot]$ means tracing out the degrees of freedom of the qubit and resonator. Performing $|e\rangle\langle e|$ and $|g\rangle\langle g|$ on $|\Phi(T_B)\rangle$ gives rise to $|\Psi\rangle = (|N0\rangle + e^{i\theta}|0N\rangle)/\sqrt{2}$ and $|\Psi\rangle = (|N0\rangle - e^{i\theta}|0N\rangle)/\sqrt{2}$, respectively. In Fig. 9, we plot the fidelity of the NOON state under various decoherence rates γ. As expected, the fidelities decline

with N. In comparing Figs. 9(a) and 9(b), the results are not sensitive to the choice of measurement basis. With a moderate decoherence rate $\gamma/g = 10^{-4}$, the fidelities are 97.9%, 95.4%, 90.1%, 85.6%, and 75.6% for $N = 1, 2, 3, 4, 5$ in Fig. 9(a) by projecting to the excited state $|e\rangle$, and they are, respectively, 97.8%, 96.0%, 92.4%, 86.9%, and 77.7% in Fig. 9(b) by measuring the ground state. Roughly the latter are slightly higher than the former and both demonstrate robustness against the environmental dissipation. Under a strong decoherence rate $\gamma/g = 10^{-3}$, however, the generation fidelity will decline to almost 50%.

V. CONCLUSION

In summary, we have presented a magnonic NOON state generation protocol based on the Floquet engineering method. The control protocol is carried out in a hybrid qubit-resonator-magnon system, where the qubit is coupled to the resonator mode with a time-modulation interaction and simultaneously coupled to two magnonic modes. Floquet engineering with the desired driving intensity, frequency, and local phases is applied to the eigen frequencies of two magnons, by which an effective time-reversal-symmetry broken Hamiltonian is constructed to realize a chiral state transfer among the resonator and the two magnonic modes. The state transfer direction could be controlled by the state of the qubit. In our protocol, when the qubit is prepared as $(|e\rangle + |g\rangle)/\sqrt{2}$, an arbitrary pure state (including the Fock state) of the resonator can thus be transferred to the two magnons at the same time. We can eventually obtain the magnonic NOON state upon a projective measurement on the qubit. We estimate the sensitivity of the state-transfer fidelity to the systematic errors in qubit-magnon coupling strength, Floquet driving intensity, frequency mismatch in magnons and qubit, and counterrotating interactions. Our protocol shows robustness against the quantum dissipation of all the components. Our work therefore provides an alternative approach to generate a NOON state in a hybrid system, which constitutes an interesting application of chiral state transfer under Floquet control.

ACKNOWLEDGMENT

[1] A. N. Boto, P. Kok, D. S. Abrams, S. L. Braunstein, C. P. Williams, and J. P. Dowling, Quantum Interferometric Optical Lithography: Exploiting Entanglement to Beat the Diffraction Limit, Phys. Rev. Lett. **85**, 2733 (2000).

[2] R. Horodecki, P. Horodecki, M. Horodecki, and K. Horodecki, Quantum entanglement, Rev. Mod. Phys. **81**, 865 (2009).

[3] L. Pezzè, A. Smerzi, M. K. Oberthaler, R. Schmied, and P. Treutlein, Quantum metrology with nonclassical states of atomic ensembles, Rev. Mod. Phys. **90**, 035005 (2018).

[4] N. Gisin and R. Thew, Quantum communication, Nat. Photonics **1**, 165 (2007).

[5] C. Bennett and B. DiVincenzo, Quantum information and computation, Nature (London) **404**, 247 (2000).

[6] F. W. Strauch, K. Jacobs, and R. W. Simmonds, Arbitrary Control of Entanglement between two Superconducting Resonators, Phys. Rev. Lett. **105**, 050501 (2010).

[7] S. T. Merkel and F. K. Wilhelm, Generation and detection of NOON states in superconducting circuits, New J. Phys. **12**, 093036 (2010).

[8] H. Wang, M. Mariantoni, R. C. Bialczak, M. Lenander, E. Lucero, M. Neeley, A. D. O'Connell, D. Sank, M. Weides, J. Wenner, T. Yamamoto, Y. Yin, J. Zhao, J. M. Martinis, and A. N. Cleland, Deterministic Entanglement of Photons in Two

Superconducting Microwave Resonators, Phys. Rev. Lett. **106**, 060401 (2011).

[9] Q. P. Su, C. P. Yang, and S. B. Zheng, Fast and simple scheme for generating NOON states of photons in circuit QED, Sci. Rep. **4**, 3898 (2015).

[10] S. J. Xiong, Z. Sun, J. M. Liu, T. Liu, and C. P. Yang, Efficient scheme for generation of photonic NOON states in circuit QED, Opt. Lett. **40**, 2221 (2015).

[11] Q.-P. Su, H.-H. Zhu, L. Yu, Y. Zhang, S.-J. Xiong, J.-M. Liu, and C.-P. Yang, Generating double NOON states of photons in circuit QED, Phys. Rev. A **95**, 022339 (2017).

[12] S.-f. Qi and J. Jing, Generating NOON states in circuit QED using a multiphoton resonance in the presence of counter-rotating interactions, Phys. Rev. A **101**, 033809 (2020).

[13] M. D'Angelo, A. Garuccio, and V. Tamma, Toward real maximally path-entangled *n*-photon-state sources, Phys. Rev. A **77**, 063826 (2008).

[14] K. Kamide, Y. Ota, S. Iwamoto, and Y. Arakawa, Method for generating a photonic NOON state with quantum dots in coupled nanocavities, Phys. Rev. A **96**, 013853 (2017).

[15] G. Vanhaele, A. Bäcker, R. Ketzmerick, and P. Schlagheck, Creating triple-NOON states with ultracold atoms via chaos-assisted tunneling, Phys. Rev. A **106**, L011301 (2022).

[16] Y. Israel, S. Rosen, and Y. Silberberg, Supersensitive Polarization Microscopy Using NOON States of Light, Phys. Rev. Lett. **112**, 103604 (2014).

[17] J. A. Jones, S. D. Karlen, J. Fitzsimons, S. C. Ardavan, A. Benjamin, A. D. Briggs, and J. J. L. Morton, Magnetic field sensing beyond the standard quantum limit using 10-spin NOON states, Science **324**, 1166 (2009).

[18] I. Afek, O. Ambar, and Y. Silberberg, High-NOON states by mixing quantum and classical light, Science **328**, 879 (2010).

[19] D. S. Grün, L. H. Ymai, K. Wittmann W., A. P. Tonel, A. Foerster, and J. Links, Integrable Atomtronic Interferometry, Phys. Rev. Lett. **129**, 020401 (2022).

[20] D. S. Grün, K. Wittmann W., L. H. Ymai, J. Links, and A. Foerster, Protocol designs for NOON states, Commun. Phys. **5**, 36 (2022).

[21] J. Zhang, M. Um, D. Lv, J.-N. Zhang, L.-M. Duan, and K. Kim, NOON States of Nine Quantized Vibrations in Two Radial Modes of a Trapped Ion, Phys. Rev. Lett. **121**, 160502 (2018).

[22] J. Chen and L. F. Wei, Deterministic generations of photonic NOON states in cavities via shortcuts to adiabaticity, Phys. Rev. A **95**, 033838 (2017).

[23] D. Lachance-Quirion, Y. Tabuchi, A. Gloppe, K. Usami, and Y. Nakamura, Hybrid quantum systems based on magnonics, Appl. Phys. Express **12**, 070101 (2019).

[24] Y. Li, W. Zhang, V. Tyberkevych, W. K. Kwok, and V. Novosad, Hybrid magnonics: Physics, circuits, and applications for coherent information processing, J. Appl. Phys. **128**, 130902 (2020).

[25] H. Yuan, Y. Cao, A. Kamra, R. A. Duine, and P. Yan, Quantum magnonics: When magnon spintronics meets quantum information science, Phys. Rep. **965**, 1 (2022).

[26] O. O. Soykal and M. E. Flatté, Strong Field Interactions between a Nanomagnet and a Photonic Cavity, Phys. Rev. Lett. **104**, 077202 (2010).

[27] O. O. Soykal and M. E. Flatté, Size dependence of strong coupling between nanomagnets and photonic cavities, Phys. Rev. B **82**, 104413 (2010).

[28] J. Li, S.-Y. Zhu, and G. S. Agarwal, Magnon-Photon-Phonon Entanglement in Cavity Magnomechanics, Phys. Rev. Lett. **121**, 203601 (2018).

[29] Y.-P. Wang, G.-Q. Zhang, D. Zhang, T.-F. Li, C.-M. Hu, and J. Q. You, Bistability of Cavity Magnon Polaritons, Phys. Rev. Lett. **120**, 057202 (2018).

[30] X. Zhang, C.-L. Zou, L. Jiang, and H. Tang, Cavity magnonmechanics, Sci. Adv. **2**, e1501286 (2016).

[31] Y. Tabuchi, S. Ishino, A. Noguchi, T. Ishikawa, R. Yamazaki, K. Usami, and Y. Nakamura, Coherent coupling between a ferromagnetic magnon and a superconducting qubit, Science **349**, 405 (2015).

[32] D. Lachance-Quirion, S. Piotr Wolski, Y. Tabuchi, S. Kono, K. Usami, and Y. Nakamura, Entanglement-based single-shot detection of a single magnon with a superconducting qubit, Science **367**, 425 (2020).

[33] Y. Tabuchi, S. Ishino, T. Ishikawa, R. Yamazaki, K. Usami, and Y. Nakamura, Hybridizing Ferromagnetic Magnons and Microwave Photons in the Quantum Limit, Phys. Rev. Lett. **113**, 083603 (2014).

[34] X. Zhang, C.-L. Zou, L. Jiang, and H. X. Tang, Strongly Coupled Magnons and Cavity Microwave Photons, Phys. Rev. Lett. **113**, 156401 (2014).

[35] S.-f. Qi and J. Jing, Generation of Bell and Greenberger-Horne-Zeilinger states from a hybrid qubit-photon-magnon system, Phys. Rev. A **105**, 022624 (2022).

[36] H. Y. Yuan, P. Yan, S. Zheng, Q. Y. He, K. Xia, and M.-H. Yung, Steady Bell State Generation via Magnon-Photon Coupling, Phys. Rev. Lett. **124**, 053602 (2020).

[37] A. Blais, A. L. Grimsmo, S. M. Girvin, and A. Wallraff, Circuit quantum electrodynamics, Rev. Mod. Phys. **93**, 025005 (2021).

[38] M. Kounalakis, G. E. W. Bauer, and Y. M. Blanter, Analog Quantum Control of Magnonic Cat States on a Chip by a Superconducting Qubit, Phys. Rev. Lett. **129**, 037205 (2022).

[39] P. Lodahl, S. Mahmoodian, S. Stobbe, A. Rauschenbeutel, P. Schneeweiss, J. Volz, H. Pichler, and P. Zoller, Chiral quantum optics, Nature (London) **541**, 473 (2017).

[40] H. Zhu, J. Yi, M.-Y. Li, J. Xiao, L. Zhang, C.-W. Yang, R. A. Kaindl, L.-J. Li, Y. Wang, and X. Zhang, Observation of chiral phonons, Science **359**, 579 (2018).

[41] A. S. Sørensen, E. Demler, and M. D. Lukin, Fractional Quantum Hall States of Atoms in Optical Lattices, Phys. Rev. Lett. **94**, 086803 (2005).

[42] J. Koch, A. A. Houck, K. L. Hur, and S. M. Girvin, Time-reversal-symmetry breaking in circuit-QED-based photon lattices, Phys. Rev. A **82**, 043811 (2010).

[43] P. Roushan, C. Neill, A. Megrant, Y. Chen, R. Babbush, R. Barends, B. Campbell, Z. Chen, B. Chiaro, A. Dunsworth, A. Fowler, E. Jeffrey, J. Kelly, E. Lucero, J. Mutus, P. ÓMalley, M. Neeley, C. Quintana, D. Sank, A. Vainsencher, *et al.*, Chiral ground-state currents of interacting photons in a synthetic magnetic field, Nat. Phys. **13**, 146 (2017).

[44] D.-W. Wang, H. Cai, R.-B. Liu, and M. O. Scully, Mesoscopic Superposition States Generated by Synthetic Spin-Orbit Interaction in Fock-State Lattices, Phys. Rev. Lett. **116**, 220502 (2016).

[45] D.-W. Wang, C. Song, W. Feng, H. Cai, D. Xu, H. Deng, H. Li, D. Zheng, X. Zhu, H. Wang, S. Zhu, and M. O. Scully, Synthesis of antisymmetric spin exchange interaction and chiral

spin clusters in superconducting circuits, Nat. Phys. **15**, 382 (2019).

[46] W. Liu, W. Feng, W. Ren, D.-W. Wang, and H. Wang, Synthesizing three-body interaction of spin chirality with superconducting qubits, Appl. Phys. Lett. **116**, 114001 (2020).

[47] N. Goldman and J. Dalibard, Periodically Driven Quantum Systems: Effective Hamiltonians and Engineered Gauge Fields, Phys. Rev. X **4**, 031027 (2014).

[48] W. Shao, C. Wu, and X.-L. Feng, Generalized James' effective Hamiltonian method, Phys. Rev. A **95**, 032124 (2017).

[49] M. Bukov, L. D'Alessio, and A. Polkovnikov, Universal high-frequency behavior of periodically driven system: From dynamical stabilization to Floquet engineering, Adv. Phys. **64**, 139 (2015).

[50] F. Petiziol, M. Sameti, S. Carretta, S. Wimberger, and F. Mintert, Quantum Simulation of Three-Body Interactions in Weakly Driven Quantum Systems, Phys. Rev. Lett. **126**, 250504 (2021).

[51] Y. Wu, L.-P. Yang, M. Gong, Y. Zheng, H. Deng, Z. Yan, Y. Zhao, K. Huang, A. D. Castellano, W. J. Munro, K. Nemoto, D.-N. Zheng, C. Sun, Y.-x. Liu, X. Zhu, and L. Lu, An efficient and compact switch for quantum circuits, npj Quantum Inf. **4**, 50 (2018).

[52] O. Kyriienko and A. S. Sørensen, Floquet quantum simulation with superconducting qubits, Phys. Rev. Appl. **9**, 064029 (2018).

[53] S. D. Liberato, C. Ciuti, and I. Carusotto, Quantum Vacuum Radiation Spectra from a Semiconductor Microcavity with a Time-Modulated Vacuum Rabi Frequency, Phys. Rev. Lett. **98**, 103602 (2007).

[54] J. Xu, C. Zhong, X. Han, D. Jin, L. Jiang, and X. Zhang, Floquet Cavity Electromagnonics, Phys. Rev. Lett. **125**, 237201 (2020).

[55] W. Wang, L. Hu, Y. Xu, K. Liu, Y. Ma, S.-B. Zheng, R. Vijay, Y. P. Song, L.-M. Duan, and L. Sun, Converting Quasiclassical States into Arbitrary Fock State Superpositions in a Superconducting Circuit, Phys. Rev. Lett. **118**, 223604 (2017).

[56] S.-f. Qi and J. Jing, Accelerated adiabatic passage in cavity magnomechanics, Phys. Rev. A **105**, 053710 (2022).

[57] A. Ruschhaupt, X. Chen, D. Alonso, and J. G. Muga, Optimally robust shortcuts to population inversion in two-level quantum systems, New J. Phys. **14**, 093040 (2012).

[58] B. Z. Rameshti, S. V. Kusminskiy, J. A. Haigh, K. Usami, D. Lachance-Quirion, Y. Nakamura, C.-M. Hu, H. X. Tang, G. E. Bauer, and Y. M. Blanter, Cavity magnonics, Phys. Rep. **979**, 1 (2022).

[59] M. Kjaergaard, M. E. Schwartz, J. Braumüller, P. Krantz, J. I.-J. Wang, S. Gustavsson, and W. D. Oliver, Superconducting qubits: Current state of play, Annu. Rev. Condens. Matter Phys. **11**, 369 (2020).

[60] B. C. Sanders, Entangled coherent states, Phys. Rev. A **45**, 6811 (1992).